INSTITUTE OF PHYSICS PUBLISHING JOURNAL OF MICROMECHANICS AND MICROENGINEERING

J. Micromech. Microeng. **16** (2006) 721–730 doi:10.1088/0960-1317/16/4/008

# Parallel micro component-to-substrate assembly with controlled poses and high surface coverage

**J Fang and K F Böhringer**

Department of Electrical Engineering, University of Washington, Box 352500, Seattle, WA 98195-2500, USA

E-mail: jdfang@ee.washington.edu and karl@ee.washington.edu

Received 13 December 2005, in final form 13 February 2006
Published 6 March 2006
Online at stacks.iop.org/JMM/16/721

**Abstract**

We demonstrate a novel parallel micro assembly process based on both shape recognition and capillary-driven self-assembly in an air environment. Mechanically diced 790 $\mu$m square silicon parts with flat or step edges were used for proof-of-concept demonstrations. Each part had only one hydrophobic 790 $\mu$m $\times$ 790 $\mu$m face and its other faces were hydrophilic. On a vibrating plate, tumbling parts were captured by cavities having an opening clearance that only admitted a single part standing vertically. The trapped parts were then transferred to a substrate having an array of receptor sites covered with water droplets. The flat-edge parts attached vertically to these sites and then capillary forces from water condensate turned them to face the substrate with their 790 $\mu$m $\times$ 790 $\mu$m hydrophilic faces. The step-edge parts attached at a tilted angle due to their featured edges and then a pressing plate laid them down. This process assembled micro parts to 1000 densely packed receptor sites in about 2 min with a defect rate of $\sim$1%. A single batch assembly process achieved 31% surface coverage, and a second batch doubled the ratio to 62%.

(Some figures in this article are in colour only in the electronic version)

## 1. Introduction

Parallel micro assembly techniques enable fast integrating and packaging of micro devices. During the past decade, several parallel micro assembly techniques have been developed and published. Based on the mechanisms to deliver and/or anchor micro components to receptor sites, these assembly techniques can be classified into four categories: (1) fluidic shape-directed self-assembly [1]; (2) capillary-driven self-assembly [2–6]; (3) electrostatically driven self-assembly [7, 8]; (4) magnetically assisted self-assembly [9]. Micro components are usually singulated in rectangular (or square) shapes from a substrate by dicing (the last fabrication step); thus, they have vertical edges, i.e., the top and bottom surfaces are geometrically identical and can therefore not be distinguished solely based on shape by any type of receptor site. In addition, a rectangle has rotational symmetry of order 2, and a square has order 4. To assemble such components, none of the above assembly techniques can effectively avoid uncertainties of face and/or in-plane orientations. Usually a micro component has electrical interconnects on a single face, so it must be mounted with unique face orientation onto a substrate to achieve electrical connections to a circuit on the substrate via flip-chip bonding. Such a component face having electrical interconnects is usually called a 'bonding face'.

Our previously reported parallel assembly techniques [10, 11], based on one- or two-stage shape recognition, required protruding pegs on parts; thus, they are not suitable for applications requiring flat part surfaces. Here we report a novel assembly process based on both shape recognition and capillary-driven mechanisms. This assembly process has the following capabilities: (1) highly dense assembly of peg-free micro components (e.g., useful for assembly of an LED display to achieve good resolution); (2) process in an air environment; (3) two controlled modes of part mounting: vertical and horizontal; (4) unique face orienting

  

of parts for horizontal mounting; (5) multi-batch assembly of various types of components, even with same dimensions; (6) high surface coverage on a substrate achieved by multi-batch assembly. With this list of capabilities available to satisfy a wide range of manufacturing requirements, applications such as micro device packaging, mass production of RFID tags and fabrication of LED displays may benefit from this parallel micro component-to-substrate assembly process. Mechanically diced 790 $\mu$m square silicon parts with a single hydrophobic face are used for the following proof-of-concept demonstrations.

## 2. Parallel assembly strategy

A typical parallel micro assembly process has two major goals: (a) micro components are delivered to receptor sites with one-to-one registration; (b) micro components contact receptor sites with their bonding faces. To achieve these assembly goals, we develop the following strategy (see figure 1, each component has one unique hydrophobic face). (1) Bulk components are distributed into apertures on an aperture plate and each aperture is occupied with exactly one vertically standing component due to geometric constraints, and the top edge of the component levels with the aperture plate surface. (2) Components from the evenly populated aperture plate are transferred onto an array of water covered receptor sites on a palletizing plate via surface tension forces, i.e., the first assembly goal is achieved and the components are vertically attached or mounted. (3) Vertically standing components are laid down to be horizontally mounted with unique face orientations, and then they self-align with the receptor sites by minimizing interfacial energies (such a capillary-driven self-alignment process can achieve sub-micron accuracy [3]). (4) Components are permanently bonded to a bonding plate via wafer level flip-chip bonding. If step (3) is skipped, then components are vertically mounted, which indicates (a) capability to achieve denser assembly with smaller footprints and (b) benefits for assembly of optical or radio frequency micro components due to the special face orientations.

## 3. Fabrication and surface treatment

During the experiments, we used two types of silicon parts (flat edge and step edge), a silicon aperture plate, a glass palletizing plate and a bonding plate.

*Flat-edge* and *step-edge silicon parts* were, respectively, fabricated by mechanical dicing from two 4 inch thermally oxidized silicon wafers with thickness of 330 $\mu$m. Before dicing, both wafers were sputter deposited with a layer of TiW/Au (50 Å/1000 Å) on a single side, and the wafer for step-edge parts underwent an extra three-step process: (1) photoresist AZ4620 was spin coated and lithographically patterned (see the appendix for the recipe) to cover an array of 590 $\mu$m squares on the side without Au; (2) exposed silicon oxide was stripped in a buffered oxide etchant (BOE) with an etching rate of ~600 Å min$^{-1}$; (3) exposed silicon was etched for 60 min by deep reactive ion etching (DRIE) to form ~190 $\mu$m deep trenches. Then the silicon wafers were mechanically diced into 790 $\mu$m square parts (figure 2). Diced parts were subsequently cleaned in acetone, isopropanol

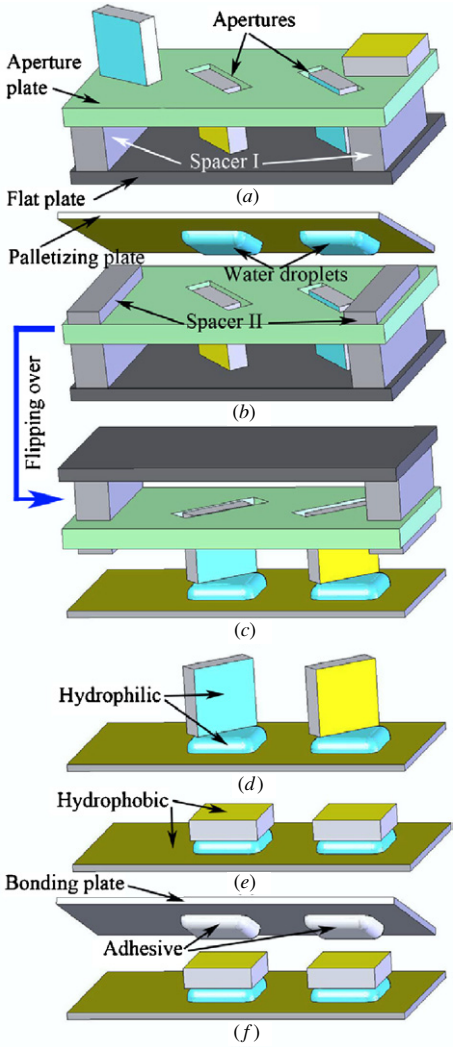


**Figure 1.** Schematic overview of the assembly process: (*a*) bulk parts fall into apertures vertically; (*b*) a palletizing plate carrying water droplets is aligned with the aperture plate; (*c*) the plates are flipped over to transfer parts onto water droplets; (*d*) parts stand on receptor sites; (*e*) parts rotate to adhere to the palletizing plate with their hydrophilic oxide faces; (*f*) parts are permanently bonded to a bonding plate via wafer level flip-chip bonding.

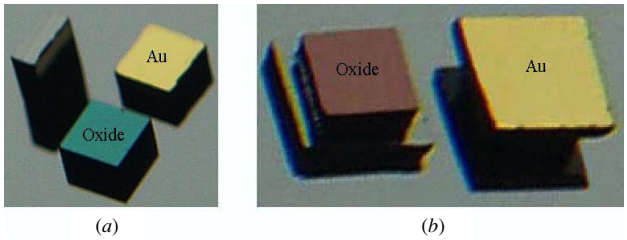


**Figure 2.** Optical images of flat-edge and step-edge parts: (*a*) top, bottom and side views of flat-edge parts (790 $\mu$m × 790 $\mu$m × 330 $\mu$m); (*b*) top and bottom views of step-edge parts (base dimension is 790 $\mu$m × 790 $\mu$m × 140 $\mu$m and top dimension is 590 $\mu$m × 590 $\mu$m × 190 $\mu$m).

(IPA) and de-ionized (DI) water in a sonicator and then collected onto a piece of filter paper and baked dry on a 100 °C hot plate for 5 min. Finally, bulk parts were soaked

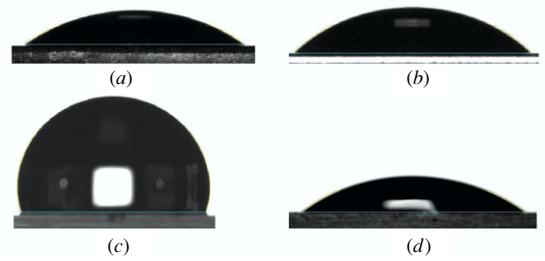


**Figure 3.** Microscope images of water droplets with different contact angles on different surfaces: (*a*) native oxide ($35^\circ \pm 3^\circ$); (*b*) thermal oxide ($45^\circ \pm 3^\circ$); (*c*) thiolated Au ($106^\circ \pm 3^\circ$); (*d*) glass ($35^\circ \pm 3^\circ$). *Note*: diced silicon parts have very limited surface areas for contact angle measurement; thus, we used large silicon substrates, which were of the same type as the substrate used to fabricate the 790 $\mu$m square parts, with different surface coatings for (*a*)–(*c*).

in a 1 mmol alkanethiol $CH_3(CH_2)_{11}SH$ solution (solvent is ethanol) overnight for a self-assembled monolayer (SAM) to selectively cover the Au surfaces. The results of water contact angle measurement using a FTA200 system (First Ten Angstroms Inc.) indicated that the thiolated Au surface was hydrophobic with a $\sim 106^\circ$ contact angle, while the other part faces with native and thermal oxide (the edges have native oxide) remained hydrophilic with contact angles of $\sim 35^\circ$ and $\sim 45^\circ$, respectively (figure 3).

A 4 inch *aperture plate* having 1000 apertures was fabricated from a 330 $\mu$m thick oxidized silicon wafer by a deep reactive ion etching (DRIE) process. First, photoresist AZ4620 was deposited and lithographically patterned on the silicon substrate. Second, a piece of dicing blue tape covered the back side of the substrate, and then the substrate was soaked in a BOE solution to completely remove exposed thermal oxide. The oxide on the back side was left to be an etch stop for the following DRIE process. Third, the substrate underwent a DRIE process for about 110 min, and then soaked in a BOE solution to remove oxide on the backside; thus, through-hole apertures were formed. Finally, photoresist was stripped with acetone, and then the substrate was cleaned in IPA and DI water.

A *glass palletizing plate* was coated with patterned thiolated Au. First, a layer of TiW/Au (50 Å/1000 Å) was sputter deposited on the glass substrate. Second, photoresist AZ1512 was spin coated and lithographically patterned to expose an array of 790 $\mu$m square gold areas. Third, exposed Au and TiW underneath were subsequently etched in an Au etchant (TFA type) and $H_2O_2$. Finally, photoresist AZ1512 was stripped with acetone and the substrate was cleaned in IPA and DI water. The cleaned substrate was soaked in a 1 mmol alkanethiol $CH_3(CH_2)_{11}SH$ solution for Au areas to become hydrophobic by adsorbing a SAM, while the exposed glass squares were used as hydrophilic (figure 3(*d*)) receptor sites.

A *glass bonding plate* was spin coated with AZ4620 and then AZ4620 was lithographically patterned to cover an array of 790 $\mu$m square bonding sites. The photoresist AZ4620 can be reflowed at $\sim 175$ °C [12] for final bonding of micro components.

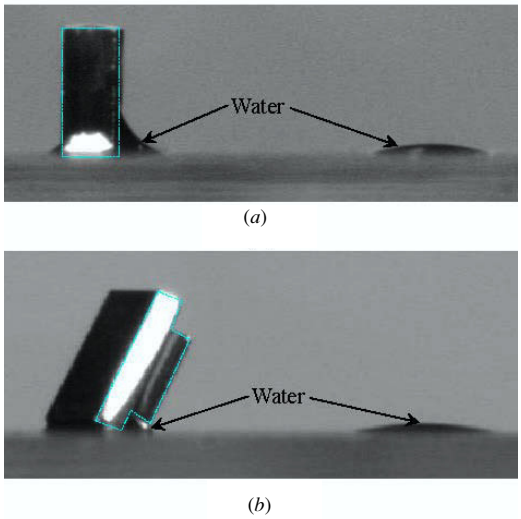


**Figure 4.** Microscopic side views of parts attached to receptor sites (the neighboring receptor sites are left unoccupied for comparison): (*a*) a flat-edge part standing vertically with its hydrophilic face to the right; (*b*) a step-edge part tilted with water gathering at the part's lower edge.

## 4. Physical modeling

Unique face orienting of micro components, shown in figure 1(*e*), is a key factor to achieve correct mounting with electrical interconnections between the substrate and the components. Microscopic views of a flat-edge silicon part and a step-edge silicon part, respectively, attached to two receptor sites by water droplets are shown in figure 4. The required conditions to lay down the flat-edge and step-edge parts with unique face orienting are, respectively, evaluated with the following two approximate physical models.

### *4.1. Flat-edge parts*

In figure 4(*a*), a flat-edge silicon part stands vertically with a significantly larger water meniscus on its right hydrophilic oxide face than its left hydrophobic Au face. Considering a part rotating about its lower right edge (shown in figure 5), in total, there are three torques on the part: a clockwise (driving) capillary torque $\tau_{cr}$ on the right face, a counterclockwise (restraining) capillary torque on left three bottom edges $\tau_{cl}$ and a counterclockwise (restraining) gravitational torque $\tau_g$. For simplicity, we consider the following situation: the part is rotating about its lower right edge for a very small angle $\alpha$ and all the water left to the axis edge enters the small gap underneath the part as shown in figure 5(*d*), which brings about a maximum possible restraining capillary torque. In the following calculations, we assume the same contact angle $\theta_c$ on all wetting surfaces.

According to the definition of a torque $\boldsymbol{\tau}$,

$$\tau = |\boldsymbol{\tau}| = |\mathbf{r} \times \mathbf{F}| = |\mathbf{r}||\mathbf{F}| \sin\theta, \tag{1}$$

where $\mathbf{F}$ and $\mathbf{r}$ are, respectively, a force vector and its moment arm vector, and $\theta$ is the intersection angle between $\mathbf{F}$ and $\mathbf{r}$. The gravitational and driving capillary torques can be, respectively, denoted by

$$\tau_g = \rho a^2 tgt/2 = \rho a^2 gt^2/2 \tag{2}$$

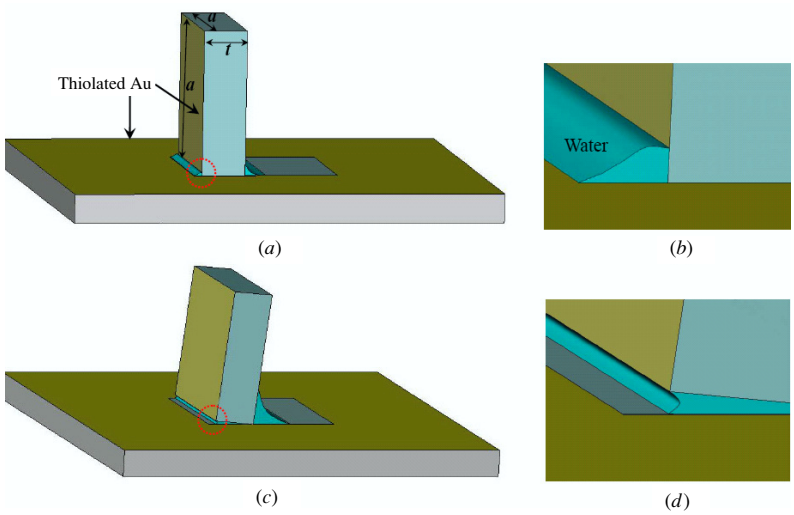


**Figure 5.** Schematic views of a vertically standing square part on a receptor site: (*a*) before steam condensation; (*b*) a zoom-in view of the circled area in (*a*); (*c*) after steam condensation (water condensate favors the hydrophilic part surface); (*d*) a zoom-in view of the circled area in (*c*).

and

$$\tau_{\mathrm{cr}} = \sigma a h_{\mathrm{w}} \sin\theta_{\mathrm{c}}, \tag{3}$$

where $\sigma$ is water surface tension, $a$, $t$ and $\rho$ are, respectively, width (or length), thickness and mass density of the part, $h_{\mathrm{w}}$ is the wetting line height on the right face and $g$ is the gravitational constant.

The capillary torque $\tau_{\mathrm{cl}}$ consists of three components, respectively, along three edges. The component along the edge parallel to the axis is given by

$$\tau_{\mathrm{cl1}} = \sigma a t \sin\theta_{\mathrm{c}}. \tag{4}$$

To calculate the other two identical torque components, respectively, along the front and back lower edges which are perpendicular to the axis, we have to integrate over the thickness of the part $t$:

$$\tau_{\mathrm{cl2}} = \int_0^t \sigma x \sin\theta_{\mathrm{c}}\, \mathrm{d}x = \sigma t^2 \sin\theta_{\mathrm{c}}/2. \tag{5}$$

Therefore, the counterclockwise capillary torque is represented by

$$\tau_{\mathrm{cl}} = \sigma t \sin\theta_{\mathrm{c}}(a + t). \tag{6}$$

The following condition must be satisfied for the part to start rotating:

$$\tau_{\mathrm{cr}} > \tau_{\mathrm{cl}} + \tau_{\mathrm{g}}. \tag{7}$$

By combining equations (2)–(7), we can calculate and obtain the minimum $h_{\mathrm{w}}$:

$$h_{\mathrm{w}} = \left[1 + \frac{\rho a^2 t g + 2\sigma t \sin\theta_{\mathrm{c}}}{2\sigma a \sin\theta_{\mathrm{c}}}\right] t. \tag{8}$$

To evaluate the minimum $h_{\mathrm{w}}$ for our fabricated flat-edge silicon parts, we plug the following values into equation (8): $\rho = 2.23$ g cm$^{-3}$, $a = 790$ $\mu$m, $t = 330$ $\mu$m, $g = 9.8$ N kg$^{-1}$, $\sigma = 72$ dyne cm$^{-1}$, $\theta_{\mathrm{c}} = 45°$. The minimum $h_{\mathrm{w}}$ is about 486 $\mu$m, which is greater than the value ~290 $\mu$m in figure 4(*a*). To raise the wetting level, we introduced steam condensation on the part surfaces (details in section 5.3).

As the part starts to rotate, the rotating continues because (1) the initially counterclockwise gravitational torque becomes less and less, and then clockwise when the center of mass goes across the axis, and (2) the capillary torques $\tau_{\mathrm{cr}}$ and $\tau_{\mathrm{cl}}$, respectively, become greater and less with an assumption of constant water volumes: as $\alpha$ increases, the wetting areas on the right face and bottom edge face of the part become greater and less, respectively, and the capillary torques are proportional to the wetting areas when the contact angle $\theta_{\mathrm{c}}$ is assumed to be constant.

### *4.2. Step-edge parts*

A step-edge part consisting of two segments, respectively, called 'base segment' and 'top segment' (the base segment is larger), stands on a receptor site in a leaning pose (edges of both segments in contact with the receptor site) rather than a vertical pose (only the edge of the base segment in contact with the receptor site) with an appropriate design, which can be derived from the following approximate physical modeling. The dimension labels $a_1, a_2, t_1, t_2$ and $w_{\mathrm{s}}$ are shown in figures 6(*b*) and (*c*).

Similar to the modeling of a flat-edge part, we consider a simple situation shown in figures 6(*b*) and (*c*): the part is rotating for a very small angle $\beta$ about the lower right edge of the base segment, and there are three torques: a clockwise (driving) capillary torque $\tau'_{\mathrm{cr}}$ along the right lower edges, a counterclockwise (restraining) capillary torque $\tau'_{\mathrm{cl}}$ along the left lower edges and a gravitational torque $\tau'_{\mathrm{g}}$.

By using the formula of the center-of-mass (COM) position for a composite object:

$$x_{\mathrm{com}} = \frac{x_1 m_1 + x_2 m_2}{m_1 + m_2}, \tag{9}$$

where $x_i$ and $m_i$ are, respectively, COM position and mass of an individual component of the object, we can calculate the COM position of the step-edge part (the coordinate origin is chosen at the segment interface, and the positive axis

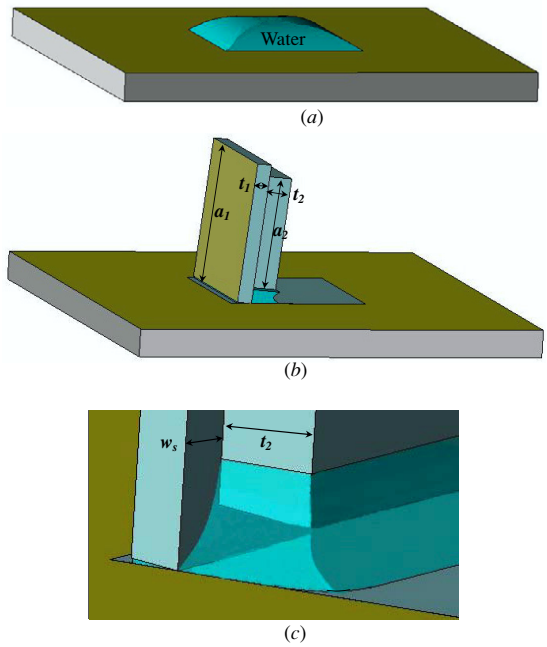


**Figure 6.** Schematic views of mounting of a step-edge part: (*a*) a receptor site covered with a water droplet; (*b*) a step-edge part in a near-vertical state; (*c*) a zoom-in view of the lower right corner of the part wetted by water.

perpendicular to the segment interface points towards the top smaller segment):

$$x_{\text{com}}^{\text{sep}} = \frac{a_2^2 t_2^2 - a_1^2 t_1^2}{2\left(a_2^2 t_2 + a_1^2 t_1\right)}. \tag{10}$$

The COM will be at the segment interface when the following relation is satisfied:

$$a_1 t_1 = a_2 t_2. \tag{11}$$

Our part design shown in figure 2(*b*) is according to equation (11); thus, the gravitational torque $\tau_{\text{g}}'$ is zero when the part starts to rotate.

Now we calculate the other two capillary torques $\tau_{\text{cl}}'$ and $\tau_{\text{cr}}'$. The situation of wetting along the three lower edges left to the axis is the same as the flat-edge part; therefore, we can write the following expression according to equation (6):

$$\tau_{\text{cl}}' = \sigma t_1 \sin\theta_{\text{c}}(a_1 + t_1). \tag{12}$$

By comparing two neighboring receptor sites in figure 4(*b*), we can find that a water droplet covers 100% of the unoccupied receptor site, and an attached step-edge part causes the water droplet to shrink its base and wet only the area directly below the step edge. For simplicity, we assume (1) wetting along the lower edges of the top segment as schematically shown in figure 6(*c*), (2) minimum wetting areas (i.e. the moment arm length is calculated from the axis to the part edge) and the same contact angle $\theta_{\text{c}}$ on all three vertical faces of the top segment. The torque component along the right lower edge of the top segment can be expressed as

$$\tau_{\text{cr1}}' = \sigma a_2 \sqrt{w_{\text{s}}^2 + t_2^2}\, \sin\left[\tan^{-1}\left(\frac{t_2}{w_{\text{s}}}\right) + \theta_{\text{c}}\right]. \tag{13}$$

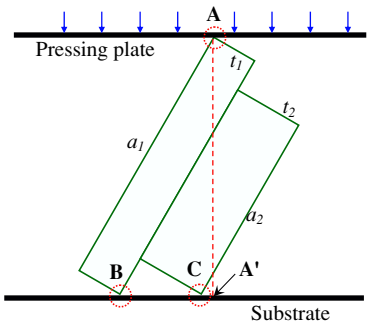


**Figure 7.** A schematic graph for a pressing plate to lay down a tilted step-edge part: the projection of point $A$ on the substrate, denoted as $A'$, must be to the right of point $C$.

The other two identical torque components, respectively, along the front and back lower edges (perpendicular to the axis) of the top segment should be integrated over the thickness $t_2$:

$$\tau_{\text{cr2}}' = \int_0^{t_2} \sigma x \cos\theta_{\text{c}}\, \mathrm{d}x = \sigma t_2^2 \cos\theta_{\text{c}}/2. \tag{14}$$

The driving capillary torque is the sum of the above three components:

$$\tau_{\text{cr}}' = \sigma a_2 \sqrt{w_{\text{s}}^2 + t_2^2}\, \sin\left[\tan^{-1}\left(\frac{t_2}{w_{\text{s}}}\right) + \theta_{\text{c}}\right] + \sigma t_2^2 \cos\theta_{\text{c}}. \tag{15}$$

The following relation must be satisfied for the step-edge part to start rotating from its vertical state:

$$\frac{\tau_{\text{cl}}'}{\tau_{\text{cr}}'} < 1. \tag{16}$$

By calculating with the following values: $\sigma = 72$ dyne cm$^{-1}$, $\theta_{\text{c}} = 45^\circ$, $a_1 = 790$ $\mu$m, $a_2 = 590$ $\mu$m, $t_1 = 140$ $\mu$m, $t_2 = 190$ $\mu$m and $w_{\text{s}} = 100$ $\mu$m, we can get the ratio of these two torques:

$$\frac{\tau_{\text{cl}}'}{\tau_{\text{cr}}'} \approx 0.67 < 1. \tag{17}$$

Equation (17) explicitly indicates that such a step-edge part cannot stand steadily in a vertical pose due to the unbalanced capillary torques. The steady state for the part is resting on its step edge in a leaning pose.

To lay down such leaning parts, we can apply a pressing plate on the top edges and parallel to the substrate (figure 7). The pressing applies a torque on the titled part, but the rotation direction depends on the projection of the contact point $A$ on the substrate, denoted as $A'$: the part stays in the leaning pose if $A'$ is between $B$ and $C$; the part is laid down if $A'$ is located to the right of $C$. For our part design, $A'$ is about 30 $\mu$m to the right of $C$.

## 5. Experimental implementation

We accomplished parallel mounting of micro components on a substrate with three major steps: positioning, orienting and bonding of micro components, i.e., bulk micro components were first distributed to an array of receptor sites, and then uniquely face oriented, and finally permanently bonded to a bonding substrate. We demonstrate a complete assembly

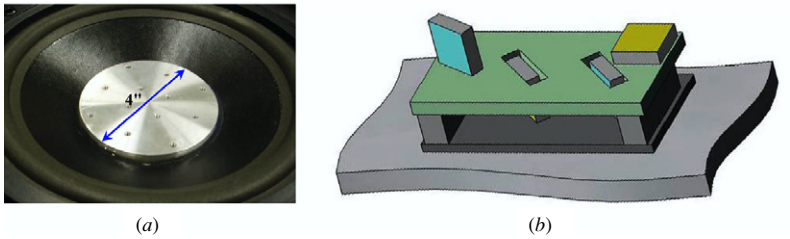


(*a*) (*b*)

**Figure 8.** Experimental setup for parts falling into apertures: (*a*) an optical image of a modified subwoofer diaphragm with a 4 inch aluminum platform mounted at the center; (*b*) schematic view of plates mounted on the vibrating aluminum platform, where parts tumble randomly until falling into apertures.

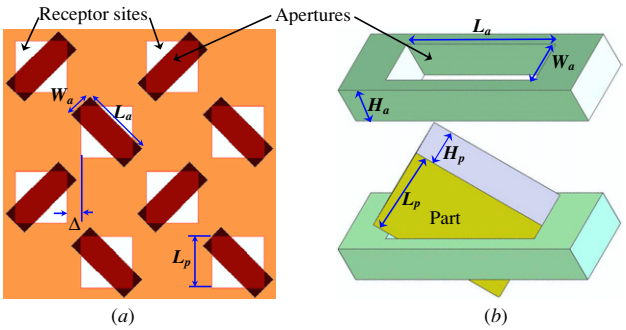


(*a*) (*b*)

**Figure 9.** Schematic design rule for parts, apertures and receptor sites: (*a*) a partial view of the overlapped layouts of the aperture plate and the palletizing plate; (*b*) a diagonally wedged part can be avoided when the aperture length $L_a$ is greater than the diagonal of the part $L_p$. We use $L_p = 790\ \mu$m, $H_p = 330\ \mu$m, $L_a = 1130\ \mu$m, $W_a = 400\ \mu$m, $H_a = 330\ \mu$m, $\Delta = 210\ \mu$m and the height of spacer I (figure 1(*a*)) $H_s = 460\ \mu$m, such that $H_s + H_a = L_p$.

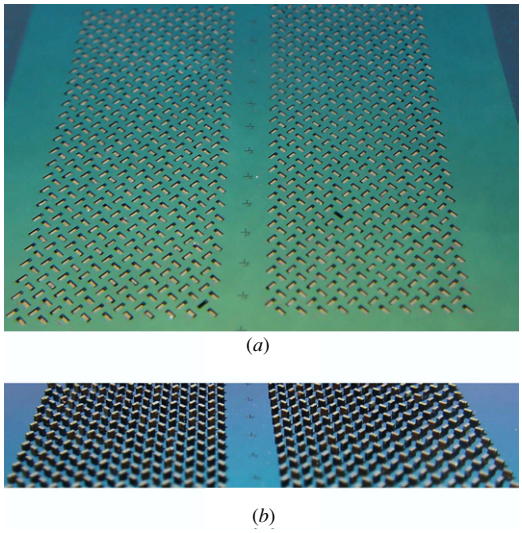

(*a*) (*b*)

**Figure 10.** Optical images of 790 $\mu$m square parts falling into apertures vertically: (*a*) an aperture plate with 1000 apertures, two apertures are empty (yield = 99.8%); (*b*) parts protruding out of the aperture plate when the spacers (figure 1(*a*)) were removed.

process for the flat-edge parts in sections 5.1–5.4. The step-edge parts share all the assembly steps with the flat-edge parts except the intermediate orienting step in section 5.3, and section 5.5 presents the special orienting step for the step-edge parts.

### *5.1. Positioning with one-to-one registration*

Bulk parts were distributed by vibration into an array of apertures. The experimental setup is shown in figure 8. The vibrating stage was a 4 inch aluminum plate glued to the center of the diaphragm of a Samson resolv 120a active subwoofer (Samson Technologies Corp., NY), and the subwoofer was driven by ac voltage signals from a function generator. The plates with 1000 apertures were mounted on the aluminum stage. When the vibrating stage was turned on, a paper funnel carrying about 3000 bulk parts was scanned across the aperture plate to dispense parts; thus, parts were uniformly fed. On the vibrating aperture plate, parts tumbled randomly until falling into the apertures. Due to geometric constraints shown in figure 9, one aperture adopted exactly one part, and the part stood vertically with a 790 $\mu$m $\times$ 330 $\mu$m footprint. The vibration amplitude was controlled to be less than 500 $\mu$m so that the trapped parts stayed in place and other free parts kept tumbling randomly until being trapped: the frequency and peak-to-peak amplitude of the sinusoidal driving voltage were, respectively, 50 Hz and 120 mV, and the volume of the subwoofer was set at level 5. Finally, redundant parts were easily wiped off since the trapped parts made a flat surface on the aperture plate. We ran the trapping experiment six times with 3000 bulk parts and observed yields ranging from 98.5% to 99.8% in about 2 min (figure 10).

### *5.2. Palletizing*

Trapped parts were then transferred to a glass palletizing plate via temporary bonding by capillary forces. The palletizing plate had an array of hydrophilic receptor sites and hydrophobic thiolated gold background. A dip coating process left water droplets on the receptor sites (figures 11(*a*) and 12(*a*)). The part transfer process is schematically shown in figures 1(*b*)–(*d*). The palletizing plate was placed on top of the aperture plate with two 150 $\mu$m thick spacers between them, and two plates were roughly aligned with $\sim$200 $\mu$m tolerance for each water droplet to oppose a part directly. These spacers prevented water droplets from contacting the hydrophilic aperture plate and parts, which must be avoided because water can cause parts to be stuck in the apertures by capillary forces (significantly greater than gravity of the 790 $\mu$m square part). When the stack of plates was flipped over, parts slid down and stood vertically on the receptor sites (figures 11(*b*) and 12(*b*)), i.e., parts have been vertically assembled.

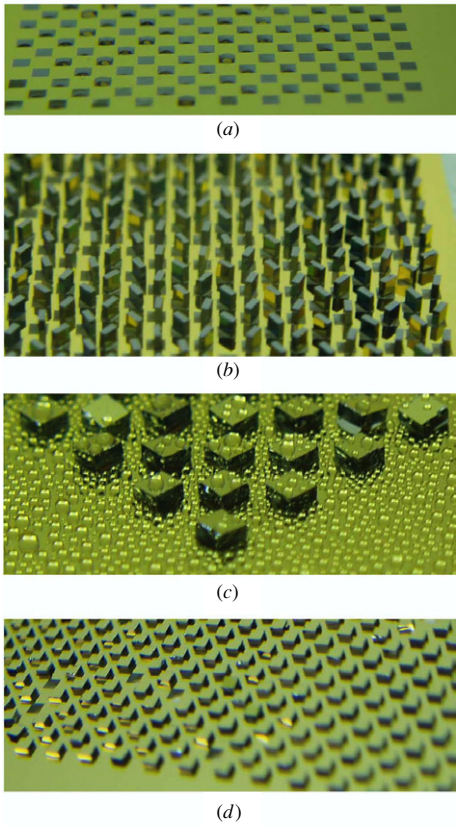

(*a*)

(*b*)

(*c*)

(*d*)

**Figure 11.** Optical images of 790 $\mu$m square parts transferred to a palletizing Pyrex plate via water droplets: (*a*) a partial view of an array of 790 $\mu$m square hydrophilic receptor sites covered with water droplets; (*b*) parts were transferred and standing vertically (see figure 1(*d*)); (*c*) water steam condensation was introduced on the palletizing plate, where steam formed film-wise and droplet-wise condensation, respectively, on hydrophilic and hydrophobic areas; (*d*) parts attached to receptor sites horizontally after steam condensation, with their only hydrophobic Au surface facing outward.

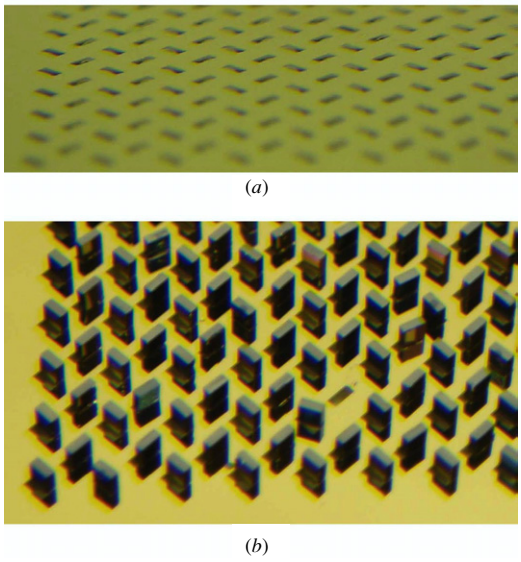

(*a*)

(*b*)

**Figure 12.** Optical images of vertically mounted 790 $\mu$m square parts: (*a*) droplets only wetted receptor sites with the same dimension as the flat edge of the parts; (*b*) parts vertically attached.

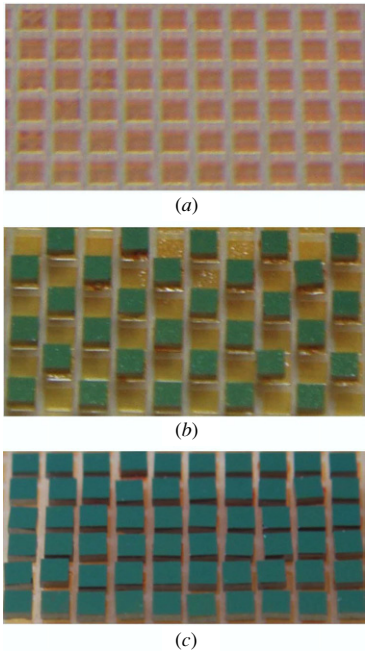

(*a*)

(*b*)

(*c*)

**Figure 13.** Permanent bonding of 790 $\mu$m square parts: (*a*) an array of bonding sites covered with photoresist AZ4620; (*b*) parts bonded by the reflowed AZ4620 after one batch transfer (figure 1(*f*)); (*c*) parts bonded by reflowed AZ4620 after second batch transfer.

### *5.3. Wet horizontal mounting with unique face orientations*

To assemble parts horizontally with 790 $\mu$m $\times$ 790 $\mu$m footprints, we introduced water steam to condense on the surfaces (droplet-wise and film-wise condensation, respectively, on hydrophobic and hydrophilic surfaces, see figure 11(*c*)); thus, the receptor sites gained more water. Since water condensate favored the hydrophilic oxide face of each part and the hydrophilic receptor sites, water wetting lines on the hydrophilic part faces were higher than those on the hydrophobic part faces. This height difference brought about a capillary torque on each part. The longer the steam condensation time, the greater the height difference and the greater the capillary torque. When the capillary torques were greater than reversely directed gravitational torques on parts, net torques drove parts to rotate to face the receptor sites with their hydrophilic oxide faces (figure 11(*d*)). A slight agitation on the palletizing plate caused parts to rotate with less water condensate because vibration brought about additional torques to overcome gravitational torques. Finally, excess water was evaporated by heating at about 70 °C and parts self-aligned with high precision to minimize interfacial energies. The less the water remained underneath the parts, the more accurate the alignment became.

### *5.4. Permanent bonding*

Finally, parts were permanently bonded to a glass bonding plate with patterned AZ4620 squares (figure 13(*a*)). When the bonding plate was in contact and aligned with the palletizing plate, parts were bonded by reflowed AZ4620. High surface coverage ratio of $\frac{1}{2}L_{\mathrm{p}}^2/(L_{\mathrm{p}}+\Delta)^2 = 31\%$ was achieved by

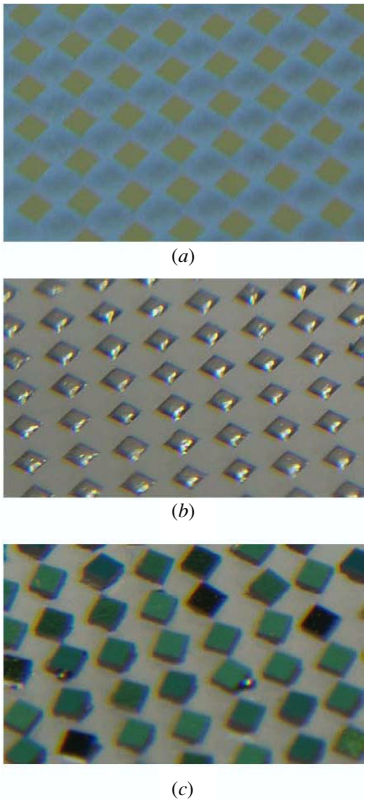

(*a*)

(*b*)

(*c*)

**Figure 14.** Optical images of parts bonded with melting solder: (*a*) an array of 790 $\mu$m square Au bonding sites on a glass substrate; (*b*) melting solder left on the Au bonding sites by a dip coating process; (*c*) parts bonded by the solder.

a single batch transfer (figure 13(*b*)). By using the same plates (aperture, palletizing and bonding plates) and offsetting the alignment between the palletizing plate and the bonding plate by a row or column ($L_p + \Delta$), a second batch transfer increased this ratio to 62% (figure 13(*c*)). Melting solder is another option for the permanent mechanical bonding together with electrical connections (figure 14), and we demonstrated this with low melting point solder (LMA-117 with a melting point of ∼47 °C; Small Parts, FL).

### *5.5. Dry horizontal mounting with unique face orientations*

Steam environment should be avoided for micro components with exposed microstructures such as cantilever beams because water residue can immobilize or even damage such fragile structures due to its surface tension force. To avoid the wet face orienting by steam condensation in section 5.3, we demonstrated a dry face-orienting process with the 790 $\mu$m square step-edge parts (figure 15): (1) the parts were attached to droplets on the receptor sites by the same method as that for the flat-edge parts and they stayed titled due to their step edges (detailed discussion in section 4.2); (2) a pressing plate laid down all the parts (the pressing plate was introduced approximately parallel to the palletizing substrate); (3) all parts self-aligned with the receptor sites to achieve interfacial energy minimization.

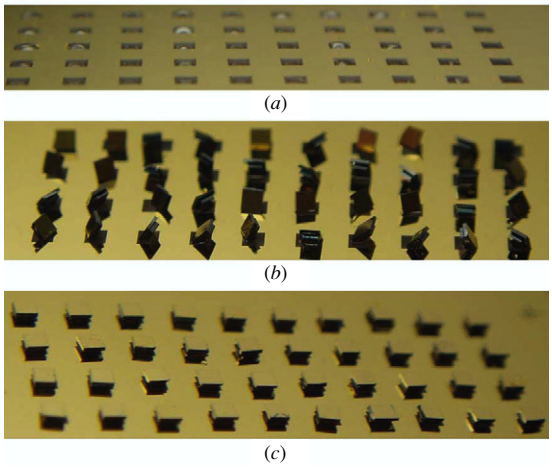

(*a*)

(*b*)

(*c*)

**Figure 15.** Optical images of the horizontal mounting of 790 $\mu$m square step-edge parts: (*a*) droplets wetting only hydrophilic receptor sites; (*b*) parts were attached to receptor sites via droplets and stayed tilted due to their step edges; (*c*) titled parts were laid down on their oxide faces by pressing.

## 6. Discussions

### *6.1. Part feeding into apertures*

Successful feeding of parts into apertures required proper vibrating of the aperture plate. Provided a constant driving voltage, the vibrating amplitude of the subwoofer diaphragm changed with the driving frequency: we ran the vibrating stage at 50 Hz to achieve proper capturing of parts; lower frequencies such as 30 Hz and 20 Hz could vibrate the captured parts out of apertures; at higher frequencies, parts kept horizontal poses due to smaller vibrating amplitude and therefore had no chances to slide into the narrow apertures. The literature [13] also reported several vibrating strategies to orient agitated parts including vertical standing.

Vibratory part feeding requires protection for fragile structures on micro electromechanical components to avoid sliding (possibly devastating) contact with apertures. Such protection can be provided by a solid frame around these fragile structures, e.g., micro structures constructed by bulk silicon etching processes.

### *6.2. Surface hydrophobicity or hydrophilicity*

In the above demonstrated assembly process, both the palletizing and wet face-orienting steps require significant contrast of water wettability for different surface areas and different part faces. Especially for the wet face-orienting step to lay down vertically standing parts, the greater the wettability contrast between the hydrophobic and hydrophilic part faces, the easier it is to accomplish this process step. The literature [14] showed that water contact angles on a silicon oxide surface increased with time, ranging from 5° to 75°, which indicates that silicon parts with fresh silicon oxide are favorable for our demonstrated assembly process.

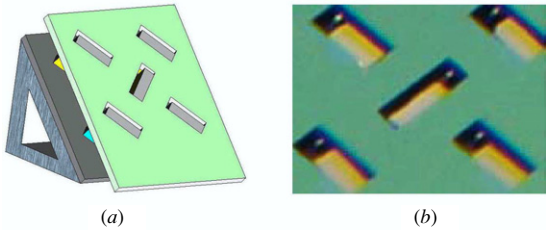

(*a*) (*b*)

**Figure 16.** Fine alignment for vertically standing parts by gravity: (*a*) schematic experimental setup; (*b*) an optical image of well-aligned parts in the apertures.

### *6.3. Fine alignment for vertically standing parts*

In case that vertically standing parts are transferred to receptor sites without droplets, i.e., no capillary forces drive the final high-precision alignment, gravity-driven fine alignment can be used before the transfer (figure 16): when the aperture plate is tilted and slightly agitated, all the trapped parts reach their lowest accessible heights inside their aperture by minimizing potential energies. After the spacers are removed, parts are protruding as shown in figure 10(*b*) and are ready for transfer.

### *6.4. Different types of liquid droplets on receptor sites*

The evaporation rate of a liquid droplet, defined as lost volume per unit time ($\mathrm{d}V/\mathrm{d}t$), is approximately proportional to the exposed surface area $S$, which can be expressed with the following equation:

$$\frac{\mathrm{d}V}{\mathrm{d}t} = k_1 S, \tag{18}$$

where $k_1$ is a constant. For a droplet with a circular base (radius $= r$) on a substrate, its exposed surface area $S$ and volume $V$ are, respectively, proportional to $r^2$ and $r^3$. Therefore, equation (18) can be rewritten as

$$\frac{\mathrm{d}V}{\mathrm{d}t} = k_2 V^{2/3} \tag{19}$$

or

$$\mathrm{d}t = k_2^{-1} V^{-2/3}\,\mathrm{d}V. \tag{20}$$

By integrating both sides of equation (20), we can obtain the total time $T$ to evaporate a whole droplet with initial volume $V_0$ and base radius $r_0$:

$$T = 3k_2^{-1} V_0^{1/3} = k_3 r_0, \tag{21}$$

where $k_2$ and $k_3$ are constants. Equation (21) indicates a proportional relationship between total evaporation time $T$ and initial base radius $r_0$ of the droplet. We observed that a water droplet on a 790 $\mu$m square glass receptor site disappeared in about 2 min under a normal lab environment and at room temperature. Air temperature and humidity also affect evaporation with warm dry air increasing evaporation and cold moist air decreasing the rate. For smaller parts, humidity and air temperature should be well controlled to achieve the complete assembly process.

Without requiring good control of humidity or air temperature, involatile liquid can be used for assembly of the step-edge parts. According to equations (12) and (15), the ratio of capillary torques in equation (17), the only determinant factor for a step-edge part to stand in a leaning pose, is independent of the surface tension of the liquid droplet. An acrylate-based liquid was tested for transferring of step-edge parts to a palletizing plate, and all the parts stayed leaning after attaching to the receptor sites. Finally, they were laid down by a pressing plate to be horizontally assembled.

## 7. Conclusions

We have demonstrated a parallel micro assembly process based on both shape recognition and capillary-driven self-assembly in an air environment, which assembled parts in a vertical or horizontal mode to densely packed receptor sites with a defect rate of ∼1%. The vertical mode is useful, e.g., for edge-emitting or vertical cavity surface-emitting laser (VCSEL) components, laser beam routing or RF MEMS components. The horizontal mode can be applied to assembly of LED displays, RFID chips and other types of flat micro components. Additionally, the multi-batch assembly capability of this assembly process enables packaging single or multiple types of micro components with high surface coverage ratios on a single substrate.

## Acknowledgments

This work is funded by NIH Center of Excellence in Genomic Science and Technology grant 1-P50-HG002360-01, with additional support from US Department of Justice award 2000-DT-CX-K001. Karl Böhringer acknowledges a fellowship from the Japan Society for the Promotion of Science. We would like to thank Xiaorong Xiong, Kerwin Wang and Rajashree Baskaran for helpful discussions, and also acknowledge Neil Bernotski for providing the vibrating stage.

## Appendix

We used the following recipe to pattern photoresist AZ4620:

(1) singe the substrate at 100 °C for 1 min;
(2) spin coat AZ4620 at 500 rpm, for 8 s, and then 1500 rpm for 40 s;
(3) bake at 70 °C for 5 min, and then 100 °C for 5 min;
(4) expose with a transparency mask for 30 s on an ABM IR aligner;
(5) develop in a solution of AZ400K:DI water = 1:2 for 1.5 min;
(6) spin dry the substrate;
(7) hard bake AZ4620 at 110 °C for 15 min.

## References

[1] Yeh H J and Smith J S 1994 Fluidic self-assembly for the integration of GaAs light-emitting diodes on Si substrates *IEEE Photon. Technol. Lett.* **6** 706–8
[2] Jacobs H O, Tao A R, Schwartz A, Gracias D H and Whitesides G M 2002 Fabrication of cylindrical display by patterned assembly *Science* **296** 323–5
[3] Srinivasan U, Liepmann D and Howe R T 2001 Microstructure to substrate self-assembly using capillary forces *IEEE J. Microelectromech. Syst.* **10** 17–24

[4] Xiong X, Hanein Y, Fang J, Wang Y, Wang W, Schwartz D T and Böhringer K F 2003 Controlled multi-batch self-assembly of micro devices *IEEE J. Microelectromech. Syst.* **12** 117–27

[5] Zheng W, Chung J H and Jacobs H O 2005 Non-robotic fabrication of packaged microsystems by shape-and-solder directed self-assembly *Proc. 18th IEEE Int. Conf. on Micro Electro Mechanical Systems (Miami Beach, FL)*

[6] Fang J, Wang K and Böhringer K F 2004 Self-assembly of micro pumps with high uniformity in performance *Proc. Solid State Sensor, Actuator, and Microsystems Workshop (Hilton Head Island, SC)* pp 208–11

[7] Böhringer K F, Goldberg K, Cohn M, Howe R T and Pisano A 1998 Parallel microassembly with electrostatic force fields *Proc. Int. Conf. on Robotics and Automation (Leuven, Belgium)*

[8] Cohn M B, Howe R T and Pisano A P 1995 Self-assembly of microsystems using non-contact electrostatic traps *Proc. ASME Int. Congress and Exposition, Symp. on Micromechanical Systems (San Francisco, CA)* pp 893–900

[9] Perkins J, Rumpler J and Fonstad C G 2002 Magnetically assisted self-assembly—a new heterogeneous integration technique *MIT Microsystems Technology Laboratories Annual Report*

[10] Fang J and Böhringer K F 2005 High yield batch packaging of micro devices with uniquely orienting self-assembly *Proc. 18th IEEE Conf. on Micro Electro Mechanical Systems (Miami, FL)* pp 12–5

[11] Fang J and Böhringer K F 2005 Uniquely orienting dry micro assembly by two-stage shape recognition *Proc. 13th Int. Conf. on Solid-State Sensors and Actuators (Seoul, Korea)* pp 956–9

[12] Pan C T, Chien C H and Hsieh C C 2004 Technique of microball lens formation for efficient optical coupling *Appl. Opt.* **43** 5939–46

[13] Swanson P J, Burridge R R and Koditschek D E 1995 Global asymptotic stability of a passive juggling strategy: a possible parts feeding method *Math. Probl. Eng.* **3** 193–224

[14] Kim S D, Shin C S, Kwak N J, Lee K B, Kwon O J and Kim C T 1997 Effects of the underlayer surface state on the interconnecting aluminum film properties *Proc. Materials Research Society Spring'97 Meeting (San Francisco, CA, 31 March–4 April)*